ORIGINAL PAPER

Multiscale failure analysis of fiber reinforced concrete based on a discrete crack model

**Guillermo Etse · Antonio Caggiano ·
Sonia Vrech**

Abstract In this work the capabilities of an interface model to predict failure behavior of steel fiber reinforced cementitious composites (SFRCCs) are evaluated at both macro and mesoscale levels of observation. The interface model is based on a hyperbolic maximum strength criterion defined in terms of the normal and shear stress components acting on the joint plane. Pre-peak regime is considered linear elastic, while the post-peak behavior is formulated in terms of the fracture energy release under failure mode I and/or II. The well-known "Mixture Theory" is adopted for modeling the interactions between fibers and the surrounding cementitious composite. The effects of both the axial forces on the fibers induced by normal relative displacements, as well as the dowel action due to tangential relative displacements in the interfaces are considered in the formulation of the interaction mechanisms between fibers and cementitious composites. After describing the interface model, this work focuses on numerical analyses of SFRCC failure behavior. Firstly, the validation analysis of the interface model is performed at the constitutive level by comparing its numerical predictions against experimental results available in scientific literature. Then, the sensitivity of the interface theory for SFRCC regarding the variation of main parameters of the composite constituents is evaluated. Finally, the attention is focused on Finite Element (FE) analysis of SFRCC failure behavior at meso and macroscopic levels of observation. The results demonstrate the capabilities of the interface theory based on the Mixture Theory to reproduce the main features of failure behavior of SRFCC in terms of fiber content and involved fracture modes.

G. Etse (✉)
Laboratory of Numerical Methods in Engineering,
CONICET and University of Buenos Aires, Buenos Aires,
Argentina
e-mail: getse@herrera.unt.edu.ar

A. Caggiano
Laboratory of Numerical Methods in Engineering,
University of Buenos Aires, Buenos Aires, Argentina
e-mail: acaggiano@fi.uba.ar

S. Vrech
CONICET and National University of Tucuman,
San Miguel de Tucuman, Argentina
e-mail: svrech@herrera.unt.edu.ar

1 Introduction

Steel fiber reinforced cementitious composites (SFRCCs), obtained by mixing short fibers and cement-based mixtures, are becoming extensively used materials in Civil Engineering applications, particularly those related to structures (Ferro et al. 2007; di Prisco et al. 2009).

Main benefits of SFRCC are the ductility improvement of structural components and the significant enhancement of residual strengths in final or cracked

stage (Barros and Figueiras 1999). The superior ductility of structures made of SFRCC, particularly in post-peak regimes, was observed under both pure mode I type of failure (Gopalaratnam and Gettu 1995) and mixed failure modes (Carpinteri and Brighenti 2010).

Several recently published experimental researches related to the mechanical characterization of SFRCC allowed to clarify relevant aspects. Among others, we refer here to the evaluations of the workability dependence on the fiber distributions by Ferrara and Meda (2006), and that of the fiber orientations on the compaction procedures by Gettu et al. (2005). Also, the work by Shannag et al. (1997) that defines the mechanisms governing the fiber pull-out behavior, and those by Buratti et al. (2011) and Tlemat et al. (2006) that analyze the post-cracking behavior of three- and four-point bending tests, respectively. Finally, it should be also noted the failure behavior evaluations of SFRCC subjected to multiaxial compressive states by Fantilli et al. (2011) and to the Brazilian test conditions by Liu et al. (1997).

A large amounts of theoretical models and numerical tools have been proposed with the aim to realistically predict the pre- and post-cracking behavior of concrete at both material and structural levels. An extended literature review of the proposed constitutive theories for modeling concrete failure behavior is given in Jirasek et al. (2000).

Concrete cracks have traditionally been treated by means of classical continuum or smeared-crack approaches in which the fracture zone is considered to be distributed in a certain region of the solid (de Borst and Guitirrez 1999). Despite its advantages from the computational point of view, classical concrete models based on the smeared crack approach suffer from strong FE-size dependence on the localization band width, see a.o. the contributions by Oliver (1989) and Rots et al. (1985). Different regularization procedures were proposed to avoid this severe deficiency of the smeared-crack approach. On the one hand, continuum models based on fracture mechanics concepts leading to fracture energy release regularization but still suffering from loss of objectivity of the deformation pattern. Fracture energy-based concrete models are, among others, due to Bazant and Oh (1983), Willam et al. (1984), Etse and Willam (1994), Shah (1990), Carpinteri et al. (1997), Comi and Perego (2001), Duan et al. (2007) and Meschke and Dumstorff (2007). On the other hand, more sophisticated constitutive theories were proposed

to solve the strong mesh dependency that appears when the governing equations turn ill posed. They are based on rate dependency, higher strain gradients, micropolar theory, etc. Among others we refer here to the contributions by Vardoulakis and Aifantis (1991), de Borst et al. (1995), Peerlings et al. (2004), Lee and Fenves (1998), Carosio et al. (2000), Etse et al. (2003), Vrech and Etse (2009), etc.

Discrete crack approaches (DCAs) aimed at incorporating strain or, moreover, displacement discontinuities into standard FE procedures have progressively became an attractive and effective alternative to the smeared-crack approach. Several proposals in the last years are currently available to introduce crack discontinuities within FE domains. It can be distinguished between the Embedded strong discontinuities (E-FEM) (Dvorkin et al. 1990; Oliver et al. 2002; Armero and Linder 2009), the eXtended Finite Element Method (X-FEM) (Wells and Sluys 2001; Liu et al. 2011), lattice model approaches (van Mier et al. 2002; Yip et al. 2006), particle models (Bazant et al. 1990; Jirasek and Bazant 1994), the hybrid-Trefftz stress-based formulation (Kaczmarczyk and Pearce 2009), the Element-free Galerkin (Belytschko et al. 1995; Singh et al. 2011) and the zero-thickness interface models (Carol et al. 1997; Dias-da Costa et al. 2010).

Among the different procedures in the framework of the discrete crack approach, the one based on zero-thickness interface elements is particularly interesting due to the simplicity of the involved numerical tools as the non-linear kinematics are fully defined in the displacement field. Recently, an interface model for SFRCC was proposed by the authors (Caggiano et al. 2012a) that includes interaction between steel fibers and concrete/mortar. Based on the interface stress-strain law for plain concrete by Carol et al. (1997), the SFRCC interface formulation by Caggiano et al. (2012a) uses the well-known "Mixture Theory" by Trusdell and Toupin (1960) to take into account the fiber-to-concrete/mortar interactions. The post-peak behavior of the interface is based on fracture energy concepts while the complex interaction between steel fibers and surrounding concrete/mortar in fracture mode I and II is considered by means of both a bond-slip model and a dowel strength based formulation, respectively.

After describing the main futures of the interface model for SFRCC, the paper focuses on the evaluation of its predictive capabilities at macro- and mesoscopic scales of observation. The results demonstrate the

sensitivity of the interface model for SFRCC to capture the influence of fundamental properties of each composite constituent as well as the interaction mechanisms between the mixture constituents. Also, the results demonstrate the accuracy of the interface model to reproduce complex failure behaviors of structural components made of SFRCC under both mode I and II types of fracture.

2 Composite material model and Mixture Theory

SFRCC is assumed to be a composite material made out of plain concrete matrix and randomly distributed fibers. The cracking behavior of SFRCC has been formulated at the interface level in terms of normal/shear stress components, $\mathbf{t}^t = [\sigma, \tau]$, related to the corresponding relative displacements, $\mathbf{u}^t = [u, v]$, representing the superscript "t" the transpose vectorial operation. The detailed description of the model, its key features and capabilities, are well documented in Caggiano et al. (2012a).

The "Mixture Theory" by Trusdell and Toupin (1960) is employed with the aim to introduce the actions of fibers in the cracking process of plain concrete. On the one hand, the bridging effect of fibers under axial stresses is explicitly considered by taking into account the bond with the surrounding concrete matrix (Caggiano and Martinelli 2012). On the other hand, their dowel action is simulated as a possible restrain of relative displacements at the two sides of the cracks in the transverse direction of fibers. The latter contribution is relevant for steel reinforcements, but can be mainly neglected for plastic fibers.

According to the basis of the Mixture Theory, the rate of the composite interface stress $\dot{\mathbf{t}}$ can be obtained as the weighted sum of the stress rates of each constituent (Oliver et al. 2008), as

$$\dot{\mathbf{t}} = w[\rho_i]\dot{\mathbf{t}}^i + \sum_{f=0}^{n_f} w[\rho_f]\left(\dot{\sigma}_f\left[\dot{\varepsilon}_N\right]\mathbf{n_N} + \dot{\tau}_f\left[\dot{\gamma}_T\right]\mathbf{n_T}\right) \tag{1}$$

being $w[\rho_\#]$ ($\# = i, f$) the weighting functions defined by means of the volume fraction $\rho_\#$ of each constituent $\#$, where i and f refer to interface and fibers, respectively; n_f the number of fibers crossing the interface; and σ_f and τ_f the bond-slip and dowel effects, respectively, of the single considered fiber which are related to the axial and tangential fiber strains, ε_N and γ_T,

respectively. They can be evaluated as $\varepsilon_N = u_N/l_f$ and $\gamma_T = u_T/l_f$, respectively, being l_f the fiber length, $u_N = \mathbf{u} \cdot \mathbf{n_N}$ the axial displacement of the single fiber, and $u_T = \mathbf{u} \cdot \mathbf{n_T}$ the transversal displacement. Thereby are $\mathbf{n_N}$ and $\mathbf{n_T}$ the unit vectors in the fiber and its normal directions, respectively.

The proposed interface formulation can be employed both in macroscopic and mesoscopic analysis of failure behaviors of SFRCC (Fig. 1). In the last case, the interface for SFRCC is used to model the behavior of all joints within the mortar while the interface formulation for plain concrete is used in all joints between mortar and aggregates.

The number of crossing fibers per interface is evaluated by means of the expression proposed by Soroushian and Lee (1990)

$$n_f = \alpha_\mathbf{N} \frac{\rho_f}{A_f} A_i \tag{2}$$

being ρ_f the fiber content, while A_f and A_i are the cross-sectional area of a single fiber and the interface area, respectively. The orientation factor was considered on the basis of the proposal given by the same authors

$$\alpha = \frac{\int_0^{\pi/2} \int_0^{\pi/2} l_f \cos\theta \cos\varpi \ d\theta d\varpi}{(\pi/2)^2 l_f} = 0.405 \tag{3}$$

being ϑ and ϖ the spatial inclination angles of the single fiber crossing the interface.

No random distribution of fibers was considered in this formulation. This could be handled within the framework of well established statistical procedures. Present interface model deals with the schemes given in Fig. 2, in which a regular iso-angular spacing between fibers crossing the interface is considered. For simplicity, it is considered that each generic fiber crosses the interface line at its mid-length, $l_f/2$.

The weighting function of Eq. (1) for plain interfaces $w[\rho_i]$ is assumed as equal to one, while $w[\rho_f]$ can be formulated as

$$w[\rho_f] = \left[1 - \alpha_f \rho_f\right]\rho_{f,1} \tag{4}$$

where $\rho_{f,1}$ is the fiber content of one single fiber, and $\left[1 - \alpha_f \rho_f\right]$ takes into account the effectiveness decay of fiber contributions on the total strength as the fiber content ρ_f increases being α_f a material parameter to be calibrated. If α_f is assumed as null, then $w[\rho_f] = \rho_{f,1}$ leading to the classical case of the "Mixture Theory". It is worth noting that $\rho_{f,1} = \frac{\rho_f}{n_f}$ and substituted into Eq. (2)

$$\rho_{f,1} = \frac{\rho_f}{n_f} = \frac{A_f}{\alpha_\mathbf{N} A_i}. \tag{5}$$

Fig. 1 Concrete specimen
(**a**), mesoscale scheme (**b**),
interfaces between
mortar-mortar and
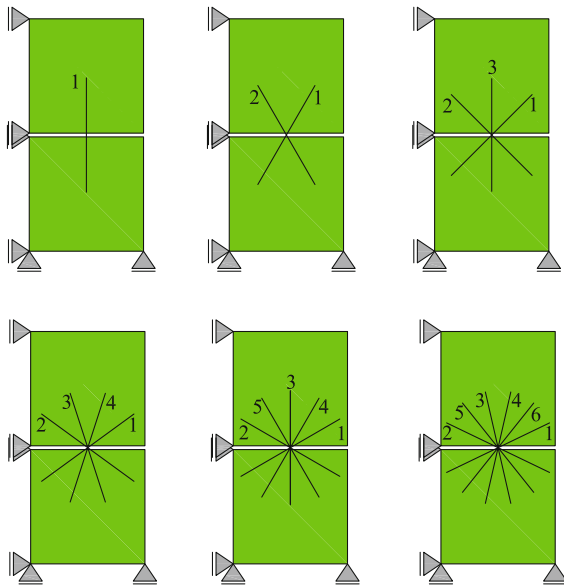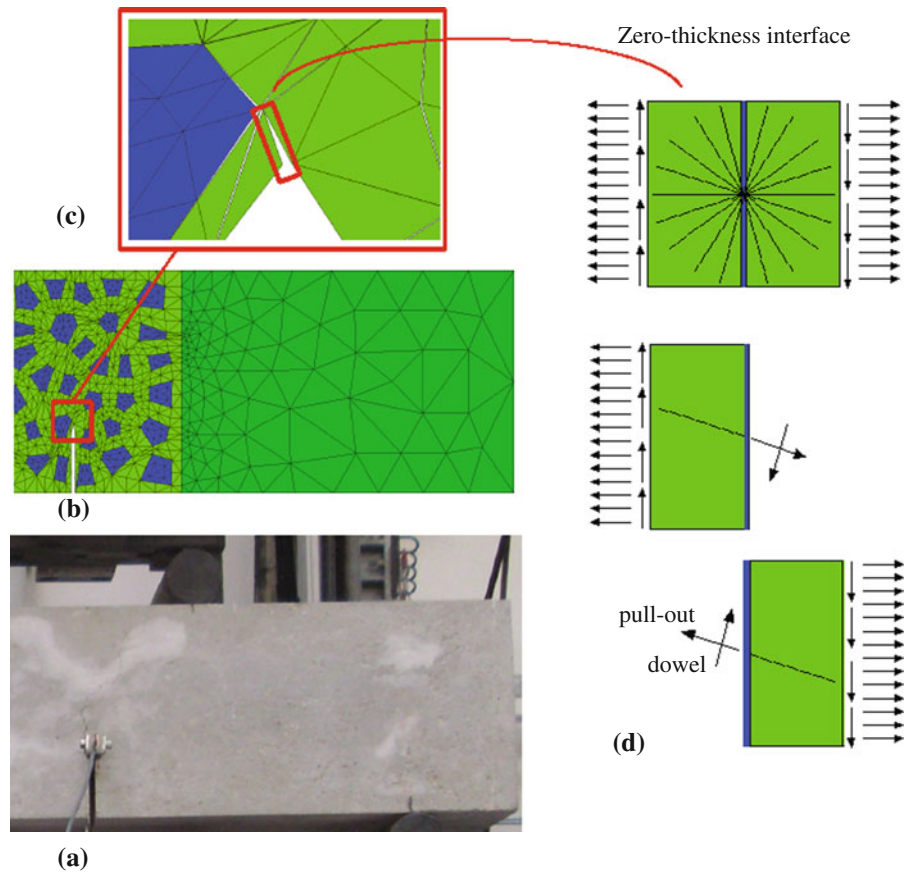mortar-aggregate (**c**) and
SFRCC interface
modeling (**d**)

Fig. 2 Considered fibers crossing the interface: as example the
cases of 1, 2, 3, 4, 5 and 6 reinforcements are presented

3 Interface model for plain concrete

The interface formulation for plain concrete in this
work was proposed by Carol et al. (1997). The con-
stitutive equations describing the failure behavior of
plain concrete interfaces are summarized in Table 1.
They are formulated in the framework of the flow the-
ory of plasticity. In table $\mathbf{C}$ represents a fully uncoupled
normal/tangential elastic stiffness operator

$$\mathbf{C} = \begin{pmatrix} k_N & 0 \\ 0 & k_T \end{pmatrix} \tag{6}$$

being k_N and k_T the normal and tangential interface
stiffnesses, respectively.

The constitutive equations in rate form result

$$\dot{\mathbf{u}} = \dot{\mathbf{u}}^{el} + \dot{\mathbf{u}}^{cr} \tag{7}$$

$$\dot{\mathbf{u}}^{el} = \mathbf{C}^{-1} \cdot \dot{\mathbf{t}}^i \tag{8}$$

$$\dot{\mathbf{t}}^i = \mathbf{C} \cdot (\dot{\mathbf{u}} - \dot{\mathbf{u}}^{cr}) \tag{9}$$

where $\dot{\mathbf{u}} = [\dot{u}, \dot{v}]^t$ is the vector of relative displacement
rates in the interface, decomposed into elastic and plas-
tic components, $\dot{\mathbf{u}}^{el}$ and $\dot{\mathbf{u}}^{cr}$, respectively. Moreover,

Table 1 Interface constitutive model for plain concrete/mortar

	Fracture—based energy formulation
Constitutive equation	$\dot{\mathbf{t}}^i = \mathbf{C} \cdot (\dot{\mathbf{u}} - \dot{\mathbf{u}}^{cr})$
	$\dot{\mathbf{u}} = \dot{\mathbf{u}}^{el} + \dot{\mathbf{u}}^{cr}$
Yield condition	$f\left(\mathbf{t}^i, \kappa\right) = \sigma_T^2 - (c - \sigma_N \tan\phi)^2 + (c - \chi \tan\phi)^2$
Flow rule	$\dot{\mathbf{u}}^{cr} = \dot{\lambda}\,\mathbf{m}$
	$\mathbf{m} = \mathbf{A} \cdot \mathbf{n}$
Cracking work evolution	$\dot{\kappa} = \dot{w}_{cr}$
	$\dot{w}_{cr} = \sigma_N \cdot \dot{u}^{cr} + \sigma_T \cdot \dot{v}^{cr}$ if $\sigma_N \geq 0$
	$\dot{w}_{cr} = \sigma_T \cdot \dot{v}^{cr}\left(1 - \frac{|\sigma_N|\tan(\phi)}{\sigma_T}\right)$ if $\sigma_N < 0$
Evolution laws	$p_i = \left[1 - (1 - r_p)\, S[\xi_{p_i}]\right] p_{0i}$
Kuhn–Tucker conditions	$\dot{\lambda} \geq 0, \quad f\left(\mathbf{t}^i, \kappa\right) \leq 0, \quad \dot{\lambda} f\left(\mathbf{t}^i, \kappa\right) = 0$
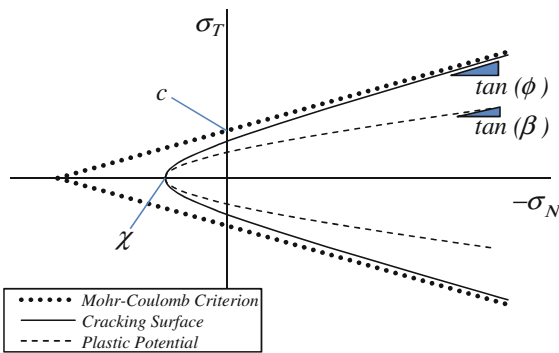
Fig. 3 Failure hyperbola by Carol et al. (1997), Mohr-Coulomb surface and plastic flow rule of the interface model

$\dot{\mathbf{t}}^i = [\dot{\sigma}_N, \dot{\sigma}_T]^t$ is the stress rate vector defined in the normal and tangential directions of the interface.

The three-parameter hyperbola of Fig. 3 defined in Carol et al. (1997) has been considered as failure criterion, $f\left(\mathbf{t}^i, \kappa\right) = 0$ which is defined in terms of the tensile strength χ, the cohesion c and the internal friction angle ϕ.

A non-associated plastic flow rule is considered whereby the gradient vector $\mathbf{m}$ defines the direction of the equivalent fracture displacements in the interface. $\mathbf{m}$ can be obtained by applying the transformation operator $\mathbf{A}$ to the gradient vector of the yield condition $\mathbf{n}$. The evolution of the yield criterion in the post-cracking regime is based on the ratio between the work spent under fracture processes in mode I and/or mixed II, w_{cr} and the corresponding fracture energies G_f^I and G_f^{IIa}, which are considered as material parameters. Thereby are:

– *Mode I type of fracture*: cracking process activates the maximum strength surface along the horizontal σ_N axis of Fig. 3;
– *asymptotic Mode II type of fracture*: cracking process is governed by shear stress under arbitrary normal stress. In case of high compressive stress, the failure criterion approaches the Mohr-Coulomb surface outlined in Fig. 3.

The evolution laws in Table 1 are valid for each internal parameter p_i of the yield condition, which are χ, c or $\tan(\phi)$. This equation defines the evolution of the internal parameter from its initial value, $p_i = p_{0i}$, to the residual one, $p_i = r_p \cdot p_{0i}$, in terms of the scaling function $S[\xi_{p_i}]$. Further details of the material formulation are given in Caggiano et al. (2012a).

4 Fiber-to-concrete interaction

Non-linear constitutive models are employed for the steel fiber characterizations. The bond-slip effect and the dowel mechanism, due to the bridging phenomenon on crack openings, are presented in this section.

4.1 Bond-slip behavior of fibers on concrete cracks

Fracture opening processes in concrete passing through fibers, activate bridging effects on both crack sides due to the fiber axial forces. The bond between fibers and concrete matrix controls this bridging effect. The axial (tensile) stresses on the fibers equal the shear stresses throughout the lateral contact surfaces of fibers embedded within the concrete matrix. Under these simplified

assumptions and considering that each generic fiber crosses the fracture line at its mid-length, $l_{emb} = l_f/2$, the following equilibrium equation can be proposed

$$\frac{d\sigma_f[x]}{dx} = -\frac{4\tau_a[x]}{d_f} \tag{10}$$

where σ_f is the fiber axial tensile stress, τ_a the local bond stress between fiber and surrounding concrete, and d_f the fiber diameter.

A bilinear shear-slip law is proposed to model the fiber-concrete debonding process as follows

$$\tau_a[x] = \begin{cases} -k_E s[x] & s[x] \leq s_e \\ -\tau_{y,a} + k_S \, (s[x] - s_e) & s_e < s[x] \leq s_u \\ 0 & s[x] > s_u \end{cases} \tag{11}$$

where $s[x]$ is defined as the tangential displacement between the fiber and concrete, at the point of the abscissa x. The positive constants k_E and k_S represent the elastic and softening slopes of such bond-slip relationships, respectively; $\tau_{y,a}$ is the shear bond strength while s_e and s_u are the elastic and ultimate slips, respectively. The complete derivation of this numerical model and its validation against bond-slip experimental tests are proposed in a previous work published by the authors, see Caggiano et al. (2011) and Caggiano et al. (2012b).

4.2 Dowel action of fibers on concrete cracks

The dowel action resulting in a shear transfer mechanism across cracks represents an important component on the overall bridging effect of steel fibers in fracture processes of SFRCC. A simple analytical model to account for the dowel action of fibers crossing cracks has been developed. It is based on the definition of the lateral force-displacement law on a generic fiber embedded in a cracked concrete matrix.

Firstly, the well-known Winkler beam theory is used to describe the dowel force, V_d, corresponding to the transversal displacement, Δ. Its analytical solution is obtained as

$$V_d = E_s J_s \lambda_f^3 \Delta \tag{12}$$

where E_s is the steel elastic modulus and J_s the fiber moment of inertia. The Winkler parameter, λ_f, is analytically derived as

$$\lambda_f = \sqrt[4]{\frac{k_c d_f}{4 E_s J_s}} = \sqrt[4]{\frac{16 k_c}{E_s \pi d_f^3}} \tag{13}$$

where k_c is the foundation (herein, the surrounding mortar) stiffness.

Finally, the empirical expression proposed by Dulacska (1972) for RC-structures is taken as the maximum dowel strength $V_{d,u}$

$$V_{d,u} = k_{dow} d_f^2 \sqrt{|f_c||\sigma_{y,s}|} \tag{14}$$

being k_{dow} a non-dimensional empirical coefficient based on the experimental results in Dulacska (1972). A typical value $k_{dow} = 1.27$ can be assumed as reference for RC-structures, see Bilal (2007). Finally, d_f is the diameter of the fiber, while f_c and $\sigma_{y,s}$ are the compressive concrete strength and the steel yield stress value, respectively.

5 Numerical analysis

In this section the interface model predictions of failure processes of SFRCC are evaluated. Firstly, the analysis compare the numerical predictions of one interface element against experimental results on SFRCC. These interface constitutive evaluations are also used to analyze the sensitivity of the interface model regarding the variation of relevant properties of the composites and their interaction mechanisms. In the second part of this section, FE discretizations at macro and mesoscopic levels of observation are used to evaluate the interface model predictions of failure behaviors of structural components made of SFRCC when they are subjected to both modes I and II type of fracture processes.

5.1 Interface model predictions of SFRCC

The analyses in this section are performed by means of two linear elastic four node FEs connected by one interface element. Therefore, the results are directly related to the interface model predictions. The FE set-up and boundary conditions of these analyses are shown in Fig. 4.

Model predictions are compared with the experimental data by Li and Li (2001). The comparisons in terms of force-displacement diagrams are shown in Figs. 5 and 6.

The considered experiments on SFRCC contain two different fiber types, namely "Dramix type I" and "type II" whose fundamental characteristics are given in Table 2. The model parameters considered
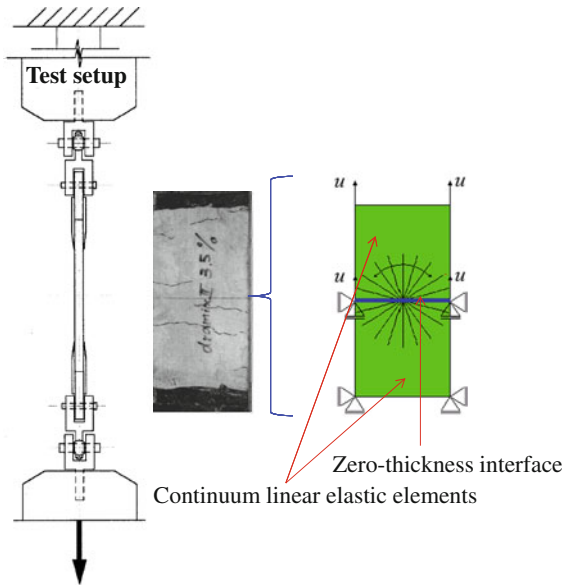
Fig. 4 FE set-up and boundary conditions for the evaluation of the experiments by Li and Li (2001) at constitutive level of the interface model. Panel dimensions according to Li and Li (2001) are $20 \times 100 \, \text{mm}^2$
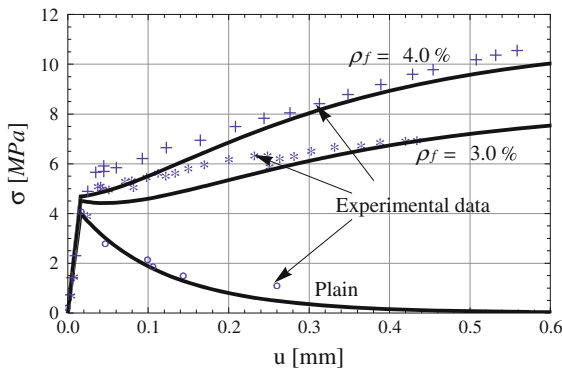

Fig. 5 Comparison between numerical predictions and experimental results by Li and Li (2001). SFRCC with "Dramix type II" fiber

Fig. 6 Comparison between numerical predictions and experimental results by Li and Li (2001). SFRCC with "Dramix type I" fiber

Table 2 Fiber types employed in the experimental tests by Li and Li (2001)

	Density (g/cm^3)	d_f (mm)	l_f (mm)	$\sigma_{y,s}$ (GPa)	E_s (GPa)
Dramix type I	7.8	0.5	30	1.20	200
Dramix type II	7.8	0.5	50	1.20	200

in these numerical analyses, adjusted according to the experimental data given in Li and Li (2001), are: $k_N = 98.75 \, \text{GPa}$, $k_T = 32.92 \, \text{GPa}$, $\tan \phi_0 = \tan \beta = \tan \phi_r = 0.6$, $\chi_0 = 4.0 \, \text{MPa}$, $c_0 = 7.0 \, \text{MPa}$, $G_f^I = 0.12 \, \text{N/mm}$, $G_f^{IIa} = 1.2 \, \text{N/mm}$. On the other hand, the parameters considered in the fiber-to-concrete interaction mechanisms are: $\tau_{y,a} = 1.95 \, \text{MPa}$, $k_E = 52.5 \, \text{MPa/mm}$ and $k_S = 1.70 \, \text{MPa/mm}$ for the bond-slip strength; $\kappa_1 = 6.5$, $f_c = 10 \cdot \chi_0$ and $k_{dow} = 0.23$ for the dowel effect.
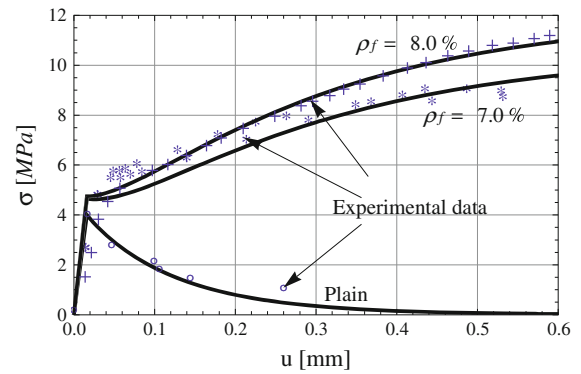
An indirect calibration procedure was performed to identify the model parameters outlined above. Particularly, denoting as **q** the set of parameters to be calibrated, the following least-square numerical procedure (similarly to the procedure in Faella et al. 2009 and Caggiano et al. 2012a) was employed

$$\bar{\mathbf{q}} = \arg \min_{\mathbf{q}} \left[\sum_{i=1}^{n} \left(\sigma_{th} \left[u_{\exp,i} ; \mathbf{q} \right] - \sigma_{\exp,i} \right)^2 \right] \quad (15)$$

being $\sigma_{th} \left[u_{\exp,i} ; \mathbf{q} \right]$ the model prediction of tensile stress, corresponding to the experimental displacement $u_{\exp,i}$ and the set of internal parameters **q**, while $\sigma_{\exp,i}$ is the corresponding experimental stress result. In Eq. (15), n represents the number of available tensile stress measurements of the considered experimental tests.

The stress-crack opening response for SFRCC with steel "Dramix type II" fiber, and fiber contents of 3.0 and 4.0 %, are given in Fig. 5. While Fig. 6 shows numerical and experimental comparisons of stress-crack opening displacements of tests on SFRCC with "Dramix type I" fiber, and fiber contents of 7.0 and 8.0 %.

The numerical predictions compared against experimental results demonstrate a very good agreement.

Fig. 7 Comparison
between the numerical
predictions of the test by Li
and Li (2001) on SFRCC
with "Dramix type II" fiber,
for full debonding strength
capacity and fracture energy
G_f^I, (**a**) 50 % of the
debonding strength and full
fracture energy G_f^I, (**b**) full
debonding strength and
50 % of G_f^I
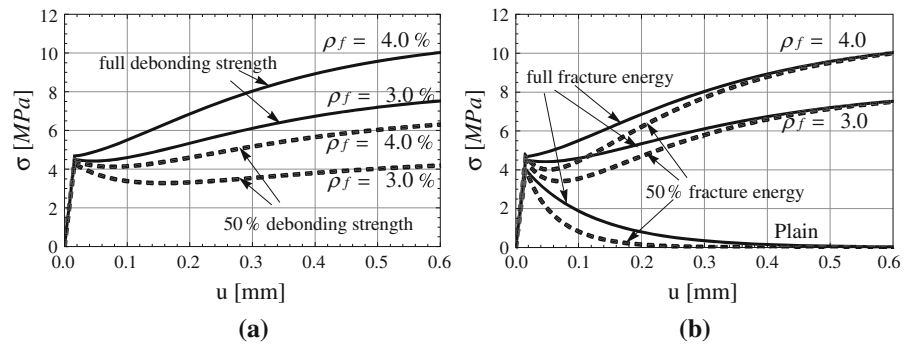
In fact, the interface model is able to realistically reproduce the overall response behaviors of SFRCC.

It should be noted that all previous numerical predictions have been obtained by just changing the fiber contents (ρ_f) and/or fiber types (changing the l_f value), according to the experimental properties. No particular calibration was required for each test.

In Fig. 7a, stress-crack opening predictions of SFRCC with steel "Dramix Type II" fiber are evaluated when full and 50 % of the debonding strength capacity of steel fibers to concrete are considered. This result clearly illustrates the capability of the interface model to realistically reproduce the incidence of the main parameter governing the interaction between concrete and steel fiber in mode I type of fracture.

In Fig. 7b the stress-crack opening behavior of the same experiment on SFRCC is illustrated, but corresponding to the case when only 50 % of the concrete fracture energy release in mode I is considered. As can be observed from Fig. 7 a, b the interface model is able to capture the influence of fundamental properties of the constituents in the overall response behavior.

Finally, the stress history on concrete panels by Hassanzadeh (1990) is evaluated as it activates failure processes under both mode I and II type of fracture. These experimental tests are performed on prismatic concrete specimens of $0.07 \times 0.07\,\text{m}^2$ cross section with a $0.015\,\text{m}$ deep notch along their perimeters. Both normal and transverse relative displacements are co-imposed on the upper border of the notched specimen while the remaining borders are fixed with the aim of reproducing the cracking processes in concrete under mode I and II types of fracture. During the first part of these tests only normal tensile displacements u are applied until the peak strength is reached. Then, tensile displacements are combined with transverse ones v defining a prefixed load angle ($\tan \theta = u/v$).

Figure 8a shows the model predictions in terms of $\sigma - u$ and $\tau - v$ curves, analyzing the case in which $\theta = \pi/6$ on both plain and SFRCC concrete panels. The proposed application considers the model parameters previously calibrated by the authors in Caggiano et al. (2012a). Numerical analyses show on the one hand, the very good agreement of the numerical prediction with the plain interface regarding the experimental results on plain concrete tests by Hassanzadeh (1990). On the other hand, the results also illustrate the significant influence of fiber reinforcements on the peak strength and post-peak ductility of the concrete panel response (when $\rho_f = 5.0\,\%$).

Figure 8b deals with the stress-crack opening predictions of SFRCC when a reduction of the 50 % of the dowel strength is considered. Model predictions mainly capture the fundamental influence of the dowel effect on the overall response behavior under mixed failure mode. As expected, the dowel effect controls the transversal interaction between concrete and steel fiber in this complex failure mode.

No experimental results are currently available in scientific literature related to the Hassanzadeh tests on FRCC. Nevertheless, the numerical results here presented, provide realistic predictions of peak stresses, ductility and post-peak behavior of FRCC tested in mixed fracture modes like the ones in the Hassanzadeh tests.

5.2 FE analysis of SFRCC at mesoscopic scale

In this section, the predictions of the interface model for SFRCC are evaluated at mesoscopic scale whereby mortar and aggregates are differentiated.

Figure 9 shows the 2-D composite geometry and the subsequent structural FE discretization employed in the present analysis. A convex polygonal representation,
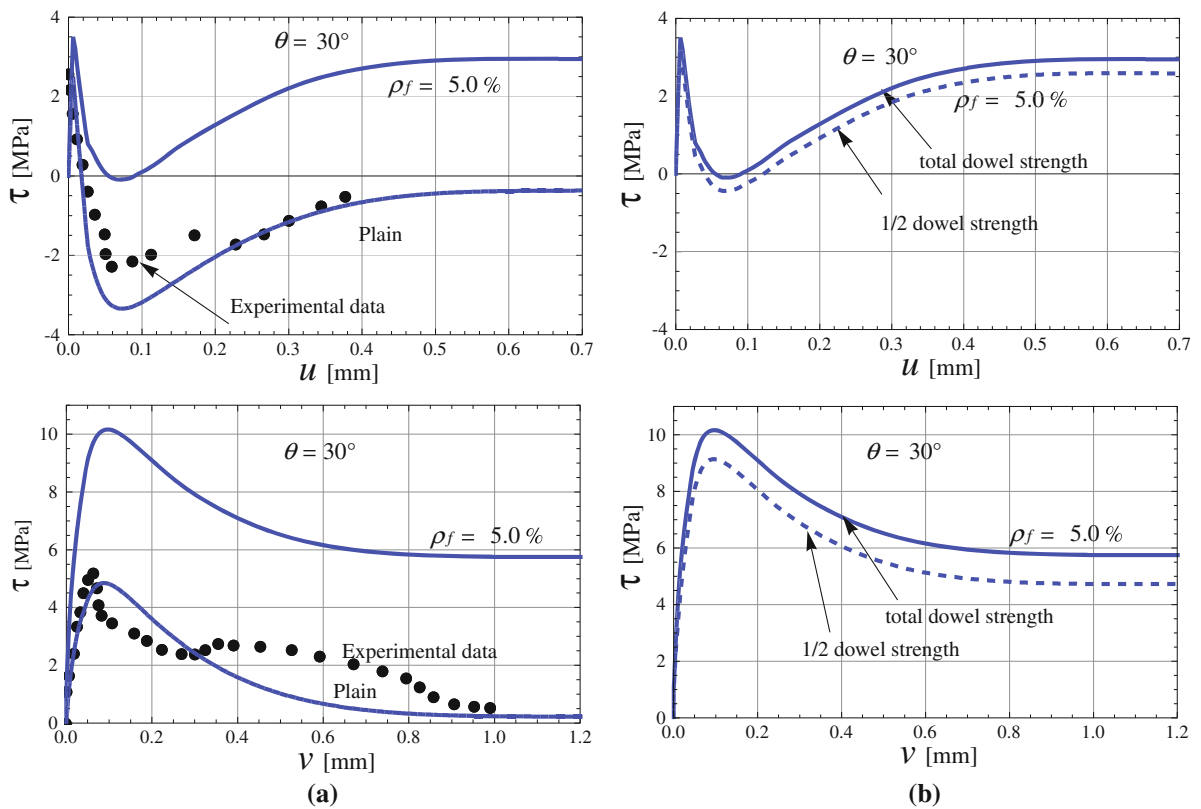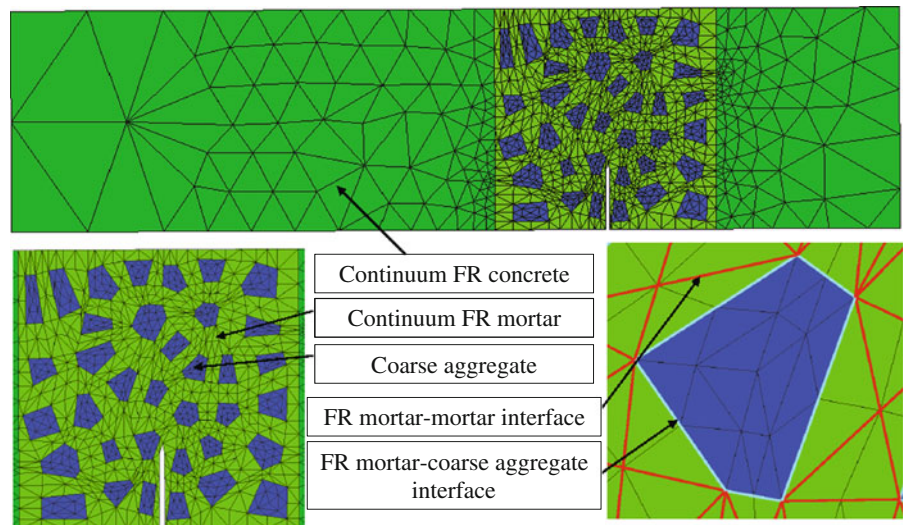
Fig. 8 **a** Experimental test by Hassanzadeh (1990) and numerical prediction for SFRCC with "Dramix type I" fiber, with $\rho_f = 5.0\%$ and, **b** effect of the dowel strength on the stress-opening displacements in mixed modes of fracture

Fig. 9 FE discretization including fiber reinforced concrete and mortar, coarse aggregates and interfaces

based on the classical Voronoi diagrams (Klein 1989), is adopted to represent the coarse aggregates present into the SFRCC mesocomposite structure. The continuum elements are assumed as linear elastic, whereas all non-linearities are concentrated within zero-thickness interface elements defined throughout the adjacent
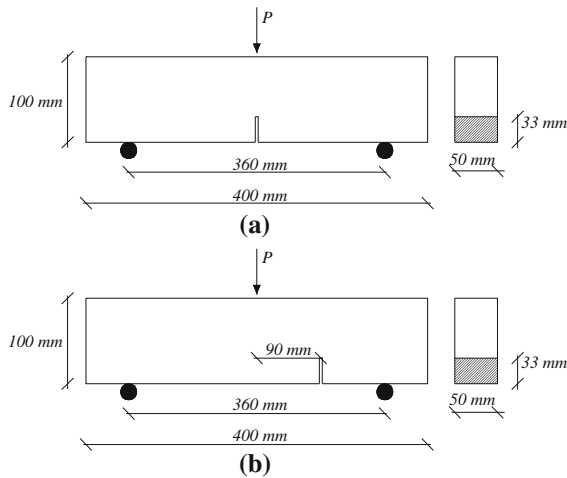
Fig. 10 Geometry and boundary conditions of the three-point bending problem of fiber reinforced concrete beam according to Carpinteri and Brighenti (2010)

edges of the finite elements. Non-linear fracture-based laws and fiber actions (in terms of both bond-slip and dowel effects) are introduced in those interface elements according to the formulation outlined in Sect. 2. In particular, aggregate-matrix interfaces do not consider the fiber effects, while fiber reinforced matrix-matrix ones take into account the contribution of passing through fibers. As can be seen in Fig. 9,

the mesoscopic discretization of the central notched portion of the beam takes into account three phases: (i) coarse aggregate, (ii) fiber reinforced mortar and (iii) interfaces. The zones with macroscopic discretizations of the beam include linear elastic elements representing the behavior of the fiber reinforced concrete located there. The elastic properties of all continuous finite elements are defined according to the "Mixture Theory" mentioned in Sect. 2. So, a generic elastic parameter is defined as

$$p_c = \rho_A p_A + \rho_M p_M + \rho_F p_F \qquad (16)$$

being p_c the elastic modulus or the Poisson's ratio. ρ_A, ρ_M and ρ_F are the volume fractions of the coarse aggregates, matrix and fibers, respectively; while p_A, p_M and p_F are the elastic parameters of each composite component.

The simulation of $50 \times 100 \times 400$ mm³ pre-cracked concrete specimens tested under three-point bending according to Carpinteri and Brighenti (2010) is performed in this section. Plane stress hypothesis and displacement-based control are assumed.

The specimens present a vertical notch (2.0 mm wide) at the bottom of the beam characterized by a depth of about 33 mm. The distance between the mid-length of the beam and the notch position varies from zero (pre-cracked beam with central notch as in

Table 3 Material parameters employed in the mesoscale analyses

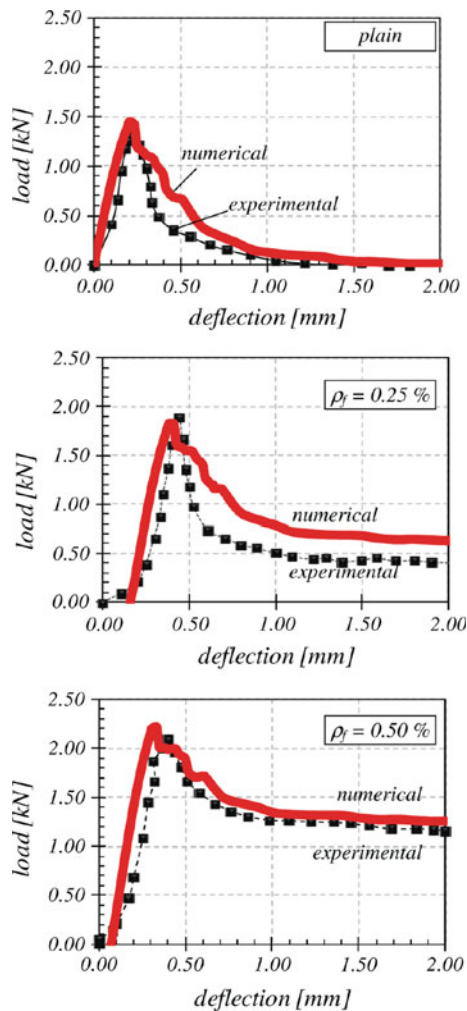|				
Continuum aggregates	ρ_A 28 %	E_A (GPa) 60.00	v_A 0.20	
Continuum mortars	ρ_M 72 %	E_M (GPa) 19.15	v_M 0.20	
Continuum fibers	ρ_F 0–0.25–0.50 %	E_F (MPa) 200.00	v_F 0.30	
Aggregate—matrix interface	k_N (MPa/mm) 1.E + 06	k_T (MPa/mm) 1.E + 06	χ_0 (MPa) 2.4	
	c_0 (MPa) 4.8	$tg\phi_0 - tg\phi_r - tg\beta$ 0.4–0.1–0.3	G_f^I (N/mm) 0.120	
	G_f^{II} (N/mm) 1.200	σ_{dil} (MPa) 10.0	α_χ −0.15	
SFRCC–SFRCC interface	k_N (MPa/mm) 1.E + 06	k_T (MPa/mm) 1.E + 06	χ_0 (MPa) 3.2	
	c_0 (MPa) 5.6	$tg\phi_0 = tg\phi_r = tg\beta$ 0.5–0.2–0.4	G_f^I (N/mm) 0.200	
	G_f^{II} (N/mm) 2.000	σ_{dil} (MPa) 10.0	α_χ −0.15	
Fiber bond-slip	$\tau_{y,a}$ (MPa) 6.95	k_E (MPa/mm) 100.0	k_S (MPa/mm) 0.1	l_f (mm) 44.0
Fiber dowel	k_{dow} 2.8	d_f (mm) 0.98	f_c' (MPa) 40.0	$\sigma_{y,s}$ (MPa) 800.0

Fig. 11 Load-deflection behavior of three-point beams with central notch. Both, plain and SFR concrete are considered. Numerical and experimental results are compared (Carpinteri and Brighenti 2010)

Fig. 10a) to 0.25*l* (pre-cracked beam with eccentrical notch as in Fig. 10b), being $l = 360$ mm the distance between the beam end supports.

The mesoscopic discretization in the notched zone of the beam allows a better simulation for following up the crack evolution. This explicit mesoscopic mesh is achieved by means of the Voronoi/Delaunay theories (Lopez 1999). It includes 36 coarse aggregates embedded in a matrix representing both fiber reinforced mortar and small aggregates. As previously indicated, two families of interfaces are considered (see Fig. 9):

– interfaces between coarse aggregate and FR matrix;
– interfaces in between fiber-reinforced cementitious mortar.

For the purpose of the numerical evaluations, three material types were considered: (1) plain concrete, (2) steel fiber reinforced concrete with fiber content $\rho_f = 0.25$ % and, (3) the same as (2) but $\rho_f = 0.50$ %. The geometry and material properties were chosen according to the tests by Carpinteri and Brighenti (2010). The mechanical parameters employed in the numerical evaluations are summarized in Table 3 (Fig. 11).

Figures 12 and 14 illustrate the cracked configurations at ultimate stages as obtained in the experimental tests by Carpinteri and Brighenti (2010) and in the numerical simulations. In both cases, failure process leads to only one macro-crack, starting at the top of the notch. Regarding the specimens with pre-fixed notch at mid-length of the beams, it can be observed that the crack evolves in an almost vertical direction (mode I type of fracture), while an inclined crack path (mixed mode of fracture) can be observed in case of eccentrical notch. Furthermore, Figs. 12 and 14 outline that the crack evolves along aggregate-matrix interfaces, which in fact represent the weakest interface in concrete composites. The numerical results confirm the predictive capacity of the interface formulation for SFRCC regarding both failure behavior and failure modes.
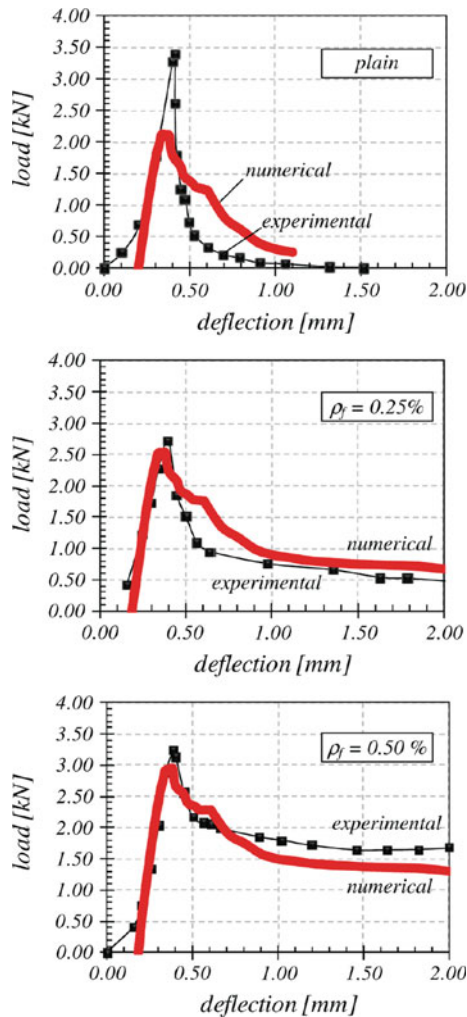
Fig. 12 Crack paths of plain concrete and SFRCC three-point bending problem with centrical notch by Carpinteri and Brighenti (2010)

Fig. 13 Load-deflection behaviors of plain concrete and SFRCC three point beams with eccentrical notch: comparison between numerical and experimental results (Carpinteri and Brighenti 2010)

Figures 11 and 13 show the force-deflection curves against corresponding experimental results. The load-displacement responses of plain concrete and SFRCC beams emphasize the significant influence of the fiber reinforcement on the peak strength and the post-peak behavior. Fiber bridging effect on cracked concrete is well captured by the considered meso-mechanical approach with non-linear joint models in all mortar-mortar and mortar-aggregate interfaces. The post-peak response of fiber-reinforced concrete is much more ductile than that of plain concrete (Fig. 14).

The comparative experimental and numerical results of the load-deflection behaviors of the beams with central and eccentrical notch show an increment of the peak load in the last case. Actually, this fact mainly occurs because the weakened cross section (pre-notched zone) in case of the beam with eccentrical notch, does not coincide with the section with maximum bending moment. However, this effect is also due to the frictional behavior of the concrete material along the fracture that it is realistically capture by the present formulation.

5.3 Macroscopic FE analysis of shear test on SFRCC

In this subsection the shear test on plain and steel reinforced mortar specimens as shown in Fig. 15 is considered. The same material parameters as in the bending problem of previous subsection are considered.

The main purpose of these analysis is to evaluate the capability of the proposed interface element to predict the failure behavior of steel reinforced mortar panels at the macroscopic level of observation when different fiber contents are considered. Non-linear interfaces are included along all contact lines between continuum finite elements in the macroscopic discretization of the mortar specimen. To assure appropriate transmission of the boundary conditions to the mortar specimen, the FE discretization includes not only the upper and lower shear frames but also the metallic shear box.

Fig. 14 Crack paths of plain concrete and SFRCC three-point beams with eccentrical notch at 0.25*l* (distance between the mid-length of the beam and the notch position) by Carpinteri and Brighenti (2010)

Fig. 15 Geometry,
boundary conditions and
discretization of the shear
tests on plain and steel
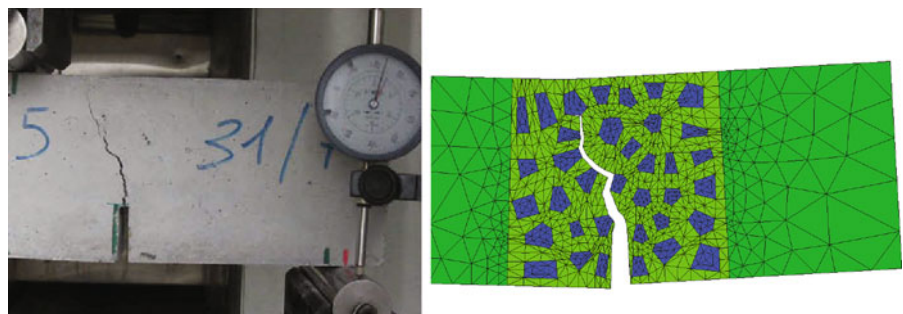reinforced mortar
specimens

Fig. 15 Geometry, boundary conditions and discretization of the shear tests on plain and steel reinforced mortar specimens
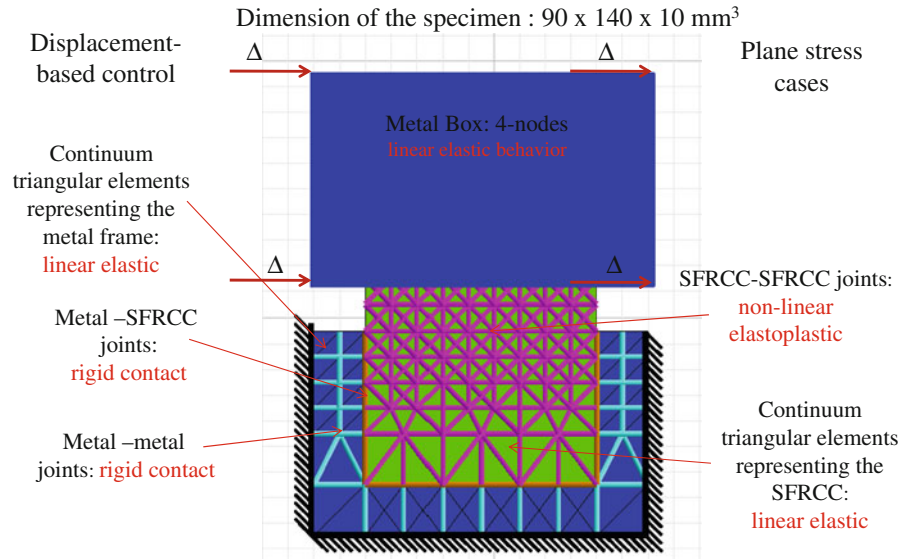
Figure 16 shows the numerical predictions of the tangential load-displacement behaviors corresponding to specimens with different fiber contents and including the plain concrete case. The increase of strength, ductility and post-peak residual strength with the fiber content is clear, while (as expected) the initial stiffness remains constant.

It is very interesting to compare the cracked configuration at final stage corresponding to the plain- and $\rho_f = 6.0\%$ fiber content mortar specimens as shown in Fig. 17. The plain mortar specimen shows a strong localization of failure in one inclined crack, normally oriented to the resulting tensile force, and followed by another, horizontally oriented crack in the middle of specimen height. In the SFRCC two inclined and less pronounced cracks can be recognized which are followed by the same horizontally oriented crack in the specimen middle.

These results demonstrate the phenomenological capabilities of the interface model to reproduce failure processes of SFRCC, when it is applied in FE discretizations along all element interfaces. Experimental studies are currently not available in literature to verify the numerical-to-experimental soundness of the proposed shear test simulation. However, the non-linear model is able to provide expected results and to reproduce the influence of the fiber content on the overall composite mechanical response.
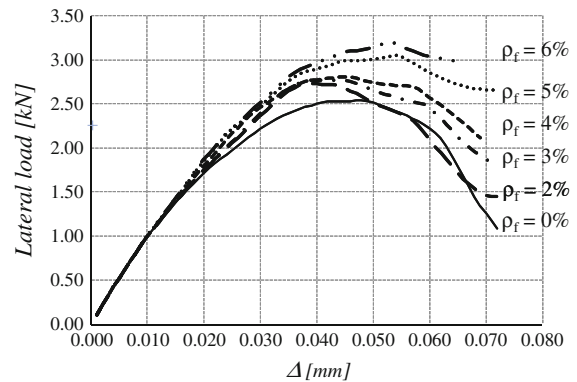

Fig. 16 Lateral load vs lateral displacements of the shear tests on plain and steel reinforced mortar specimens

6 Conclusions

In this work the predictive capabilities of a discontinuous approach for failure analyses of steel fiber reinforced cementitious composite have been evaluated at different levels of observation. The constitutive model considers the well-known "Mixture Theory" to simulate the combined bridging interactions of fibers in concrete/mortar cracks. Particularly, the interactions between steel fibers and concrete matrix, associated with debonding and dowel effects, are explicitly considered in the interface constitutive formulation.

Fig. 17 Final pattern of the **a** plain mortar and **b** steel fiber reinforced mortar ($rho_f = 6.0\%$ fiber content) specimens after the numerical analyses with the *shear box*

(a)   (b)
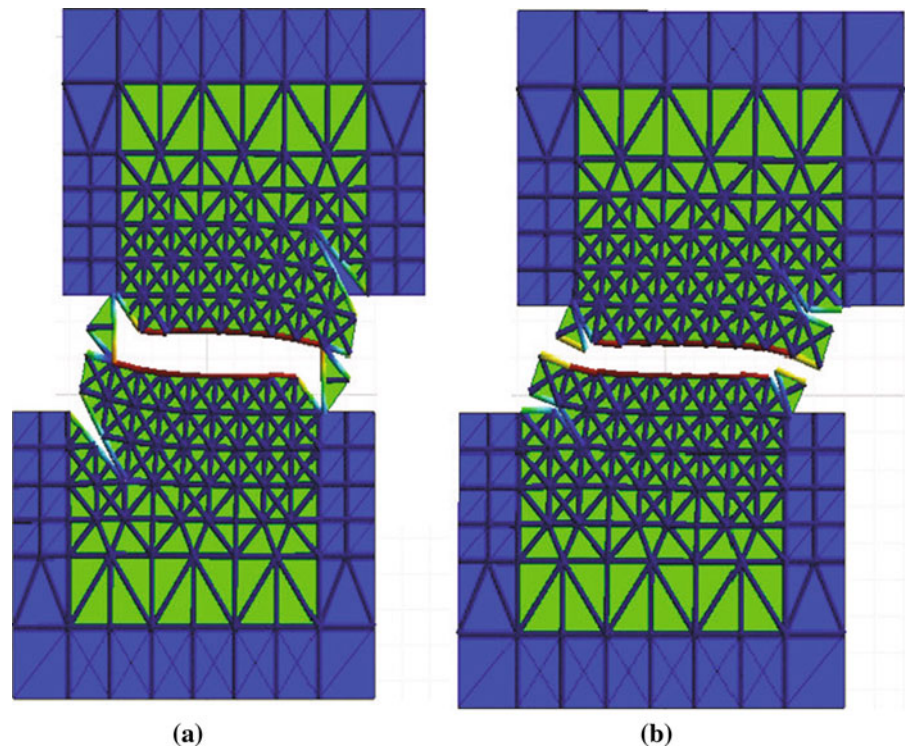
The discrete crack formulation was employed to simulate the fracture behavior of SFRCC at constitutive, mesoscopic and macroscopic levels of observations.

The numerical results in this paper demonstrate that the discontinuous approach based on non-linear interface formulation leads to realistic predictions of failure processes of SFRCC under different load scenarios and considering a wide spectrum of fiber contents. The interfaces provide accurate results of failure behaviors when they are considered both in mesoscopic and macroscopic FE discretizations of concrete and mortar components. The model is able to capture the significant influence of the steel fiber content on the maximum strength and post-peak ductility in mode I and mixed mode of failure showing the capability of the interface formulation to capture the complex interaction mechanisms between fibers and concrete/mortars.

References

Armero F, Linder C (2009) Numerical simulation of dynamic fracture using finite elements with embedded discontinuities. Int J Fract 160:119

Barros J, Figueiras J (1999) Flexural behavior of SFRC: testing and modeling. ASCE J Mater Civil Eng 11(4):331

Bazant Z, Oh B (1983) Crack band theory for fracture of concrete. Mater Struct 16:155

Bazant Z, Tabbara M, Kazemi M, Pijaudier-Cabot G (1990) Random particle model for fracture of aggregate or fiber composites. ASCE JEM 116:1686

Belytschko T, Lu Y, Gu L (1995) Crack propagation by element-free Galerkin methods. Eng Fract Mech 51(2):295

Bilal E-A (2007) Behavior of beams with dowel action. Eng Struct 29(6):899

Buratti N, Mazzotti C, Savoia M (2011) Post-cracking behaviour of steel and macro-synthetic fibre-reinforced concretes. Constr Build Mater 25:2713

Caggiano A, Etse G, Martinelli E (2011) Interface model for fracture behaviour of fiber-reinforced cementitious composites (FRCCs): theoretical formulation and applications. Eur J Environ Civil Eng 15(9):1339

Caggiano A, Etse G, Martinelli E (2012a) Zero-thickness interface model formulation for failure behavior of fiber-reinforced cementitious composites. Comput Struct 9899(0):23

Caggiano A, Martinelli E, Faella C (2012b) A fully-analytical approach for modelling the response of FRP plates bonded to a brittle substrate. Int J Solids Struct 49(17):2291–2300

Caggiano A, Martinelli E (2012) A unified formulation for simulating the bond behaviour of fibers in cementitious materials. Mater Des. doi:10.1016/j.matdes.2012.05.003

Carol I, Prat P, Lopez C (1997) Normal/shear cracking model: applications to discrete crack analysis. ASCE JEM 123:765

Carosio A, Willam K, Etse G (2000) On the consistency of viscoplastic formulations. Int J Solids Struct 37(48–50):7349

Carpinteri A, Brighenti R (2010) Fracture behaviour of plain and fiber-reinforced concrete with different water content under mixed mode loading. Mater Des 31:2032

Carpinteri A, Chiaia B, Nemati KM (1997) Complex fracture energy dissipation in concrete under different loading conditions. Mech Mater 26(2):93

Comi C, Perego U (2001) Fracture energy based bi-dissipative damage model for concrete. Int J Solids Struct 38(36–37):6427

de Borst R, Guitirrez M (1999) A unified framework for concrete damage and fracture models including size effects. Int J Fract 95:261

de Borst R, Pamin J, Peerlings R, Sluys L (1995) On gradient-enhanced damage and plasticity models for failure in quasi-brittle and frictional materials. Comput Mech 17:130

Dias-da Costa D, Alfaiate J, Sluys L, Jlio E (2010) A comparative study on the modelling of discontinuous fracture by means of enriched nodal and element techniques and interface elements. Int J Fract 161:97

di Prisco M, Plizzari G, Vandewalle L (2009) Fibre reinforced concrete: new design perspectives. Mater Struct 42:1261

Duan K, Hu X, Wittmann FH (2007) Size effect on specific fracture energy of concrete. Eng Fract Mech 74(1–2):87

Dulacska H (1972) Dowel action of reinforcement crossing cracks in concrete. ACI Struct J 69(12):754

Dvorkin E, Cuitino A, Gioia G (1990) Finite elements with displacement embedded localization lines insensitive to mesh size and distortions. Int J Numer Methods Eng 30:541

Etse G, Nieto M, Steinmann P (2003) A micropolar microplane theory. Int J Eng Sci 41(13–14):1631

Etse G, Willam K (1994) A fracture energy-based constitutive formulation for inelastic behavior of plain concrete. ASCE-JEM 120:1983

Faella C, Martinelli E, Nigro E (2009) Direct versus indirect method for identifying FRP-to-concrete interface relationships. J Compos Constr 13(3):226

Fantilli A, Vallini P, Chiaia B (2011) Ductility of fiber-reinforced self-consolidating concrete under multi-axial compression. Cem Concr Compos 33:520

Ferrara L, Meda A (2006) Relationships between fibre distribution, workability and the mechanical properties of SFRC applied to precast roof elements. Mater Struct 39:411

Ferro G, Carpinteri A, Ventura G (2007) Minimum reinforcement in concrete structures and material/structural instability. Int J Fract 146:213

Gettu R, Gardner D, Saldvar H, Barragn B (2005) Study of the distribution and orientation of fibers in SFRC specimens. Mater Struct 38:31

Gopalaratnam VS, Gettu R (1995) On the characterization of flexural toughness in fiber reinforced concretes. Cem Concr Compos 17(3):239

Hassanzadeh M (1990) Determination of fracture zone properties in mixed mode I and II. Eng Fract Mech 35(4–5):845

Jirasek M, Bazant ZP (1994) Macroscopic fracture characteristics of random particle systems. Int J Fract 69:201

Jirasek M (2000) Comparative study on finite elements with embedded discontinuities. Comput Methods Appl Mech Eng 188(1–3):307

Kaczmarczyk L, Pearce CJ (2009) A corotational hybrid-Trefftz stress formulation for modelling cohesive cracks. Comput Methods Appl Mech Eng 198(15–16):1298

Klein R (1989) Concrete and abstract Voronoi diagrams. Lecture notes in computer science, Springer, Berlin

Lee J, Fenves G (1998) Plastic-damage model for cyclic loading of concrete structures. ASCE JEM 124(8):892

Li F, Li Z (2001) Continuum damage mechanics based modeling of fiber reinforced concrete in tension. Int J Solids Struct 38(5):777

Liu C, Lovato M, Stout M, Huang Y (1997) Measurement of the fracture toughness of a fiber-reinforced composite using the Brazilian disk geometry. Int J Fract 87:241

Liu Z, Menouillard T, Belytschko T (2011) An XFEM/spectral element method for dynamic crack propagation. Int J Fract 169:183

Lopez C (1999) Microstructural analysis of concrete fracture using interface elements. Application to various concretes (in Spanish). Ph.D. thesis, Universitat Politecnica de Catalunya, ETSECCCP-UPC

Meschke G, Dumstorff P (2007) Energy-based modeling of cohesive and cohesionless cracks via X-FEM. Comput Methods Appl Mech Eng 196(21–24):2338

Oliver J (1989) Consistent characteristic length for smeared cracking models. Int J Numer Methods Eng 28:461

Oliver J, Huespe A, Pulido M, Chaves E (2002) From continuum mechanics to fracture mechanics: the strong discontinuity approach. Eng Fract Mech 69:113

Oliver J, Linero D, Huespe A, Manzoli O (2008) Two-dimensional modeling of material failure in reinforced concrete by means of a continuum strong discontinuity approach. Comput Methods Appl Mech Eng 197(1):332

Peerlings R, Massart T, Geers M (2004) A thermodynamically motivated implicit gradient damage framework and its application to brick masonry cracking. Comput Methods Appl Mech Eng 193(30–32):3403

Rots J, Nauta P, Kusters G, Blaauwendraad J (1985) Smeared crack approach and fracture localization in concrete. Heron 30:1

Shah S (1990) Size-effect method for determining fracture energy and process zone size of concrete. Mater Struct 23:461

Shannag J, Brincker R, Hansen W (1997) Pullout behavior of steel fibers from cement-based composites. Cem Concr Res 27:925

Singh I, Mishra B, Pant M (2011) An enrichment based new criterion for the simulation of multiple interacting cracks using element free Galerkin method. Int J Fract 167:157

Soroushian P, Lee C (1990) Distribution and orientation of fibers in steel fiber reinforced concrete. ACI Mater J 87(5):433

Trusdell C, Toupin R (1960) The classical field theories, the classical field theories, Handbuch der Physik, vol III/I. Springer, Berlin

Tlemat H, Pilakoutas K, Neocleous K (2006) Stress-strain characteristic of SFRC using recycled fibres. Mater Struct 39: 365

Vardoulakis I, Aifantis EC (1991) A gradient flow theory of plasticity for granular materials. Acta Mech 87:197

van Mier J, van Vliet M, Wang T (2002) Fracture mechanisms in particle composites: statistical aspects in lattice type analysis. Mech Mater 34:705

Vrech S, Etse G (2009) Gradient and fracture energy-based plasticity theory for quasi-brittle materials like concrete. Comput Methods Appl Mech Eng 199(1–4):136

Wells G, Sluys L (2001) A new method for modelling cohesive cracks using finite elements. Int J Numer Methods Eng 50:2667

Willam K, Bicanic N, Sture S (1984) Constitutive and computational aspects of strain-softening and localization in solids. In: Willam K (ed) Constitutive equations: micro, macro and computational aspects, ASME-WAM84, New Orleans, Symposium, vol G00274, New York, pp 233–252

Yip M, Li Z, Liao BS, Bolander J (2006) Irregular lattice models of fracture of multiphase particulate materials. Int J Fract 140:113